Condensation transition and drifting condensates in the accelerated exclusion process

Ori Hirschberg[1,2] and David Mukamel[2]

[1] *Department of Physics, Technion, 3200003 Haifa, Israel*
[2] *Department of Physics of Complex Systems, Weizmann Institute of Science, 76100 Rehovot, Israel*

(Dated: October 9, 2015)

Recently, it was shown that spatial correlations may have a drastic effect on the dynamics of real-space condensates in driven mass-transport systems: in models with a spatially correlated steady state, the condensate is quite generically found to drift with a non-vanishing velocity. Here we examine the condensate dynamics in the accelerate exclusion process (AEP), where spatial correlations are present. This model is a "facilitated" generalization of the totally asymmetric simple exclusion process (TASEP) where each hopping particle may trigger another hopping event. Within a mean-field approach that captures some of the effects of correlations, we calculate the phase diagram of the AEP, analyze the nature of the condensation transition, and show that the condensate drifts, albeit with a velocity that vanishes in the thermodynamic limit. Numerical simulations are consistent with the mean-field phase diagram.

arXiv:1510.02222v1 [cond-mat.stat-mech] 8 Oct 2015

I. INTRODUCTION

A traffic jam forms on a highway; a macroscopically linked hub develops in a complex network; marbles in a shaken compartmentalized box cluster in a single compartment; a finite fraction of the capital in a macroeconomic system is held in the hands of few agents. These varied phenomena can all be described as types of *real-space condensation*, where a macroscopic fraction of some "mass" (cars, links, marbles, capital, etc.) is typically concentrated in a microscopic part of the system [1–6]. Condensation in such systems usually sets in via a phase transition which is mathematically similar to Bose-Einstein condensation: at low densities the system is in a homogenous disordered phase, and when the density is increased beyond a critical value a condensate forms. Such condensation transitions occur both in and out of equilibrium, and their static and dynamical properties have received much attention in recent years [7–22].

The study of such condensation transitions is simplest in exactly solvable models. The most notable examples of models of this type are zero-range processes (ZRPs) [1–3]. These are models of transport in which particles hop stochastically among sites with rates that depend only on the occupation number of the departure site. In this class of models, the steady-state distribution factorizes into a product of single site terms and can ba calculated exactly. Therefore, one may analyze the precise conditions under which condensation takes place in a ZRP [8]. ZRPs have been used to model condensation in a variety of contexts, including the examples of condensing systems listed in the opening lines of this paper [23–26].

In generic systems, the steady-state distribution is not known and exact results about condensation are scarce. In some specific models, the problem can by bypassed by specially tailored methods which allow one to study condensation [7, 27, 28]. However, in most cases, exact methods for the analysis of condensation are not available. In these cases, one usually resorts to approximate methods such as mean-field (MF) approximations, where correlations between sites are neglected. Although inexact, MF methods often lead to a qualitative description of the collective behavior of the model, and thus provide insight into the phenomena under study. Usually, MF descriptions not only neglect correlations among sites, but also assume that the system is homogeneous. Thus, one studies condensation in the model under consideration by effectively describing it as a ZRP.

One drawback of such MF methods is that they do not adequately describe the condensed phase. This phase is not homogeneous, as the formation of a condensate breaks translational invariance, and usual MF treatments ignore such inhomogeneities. Recently, a MF method was proposed which is better suited for the study of the inhomogeneity of the condensed phase [29]. In a nutshell, different sites are assumed in this MF scheme to be independent but not necessarily identically distributed. The occupation probability of a site is thus allowed to depend on its distance from the condensate.

An important aspect of condensing systems which is modified by the presence of spatial correlations concerns the dynamics of the condensate. In the ZRP, the condensate location remains static for long periods of time (the duration of which diverges with the system size faster than quadratically), until a fluctuation eventually leads the condensate to relocate [30]. When it relocates it does so to a random site. In Ref. [29] it was shown, using the aforementioned modified MF method, that spatial correlations in the steady state often modify this condensate dynamics: they may lead the condensate to drift along the system with a non-zero velocity in any finite system size. The dynamics of condensates is currently an active line of study, as condensing systems provide one of the simplest settings in which collective and emergent motion can be studied [30–38]

In the present paper, we demonstrate the use of the MF method of Ref. [29] by applying it to the study of condensation in a recently introduced accelerated exclusion process (AEP) [39]. This model is a "facilitated" version of the well known totally asymmetric simple exclusion process (TASEP), in which a particle hop may

trigger a second (simultaneous) hop, see below. Numerical and analytical studies of finite AEP systems and of some specific infinite-system limits have suggested that a condensation phase transition occurs in the model. However, lacking an analytical description of the steady state, the conditions for the occurrence of this apparent phase transition in the thermodynamic limit were not known. A subsequent mean-field study of the model was useful in clarifying its behavior in the homogeneous disordered phase, but did not resolve the questions regarding the phase transition [40] (see Refs. [41, 42] for studies of related models). Here, using the MF scheme of Ref. [29], we calculate the MF phase diagram of the model and explain some of the numerical findings of Ref. [39]. Furthermore, Our analysis suggests that the model has a drifting condensate, and thus the AEP provides another example for the condensate-drift mechanism studied in Ref. [29].

The paper is organized as follows. We begin in Sec. II by defining the model. Two representations are presented: the original definition of Ref. [39], and an alternative description in which similarities of the model to a ZRP are more apparent. After summarizing the main results of the paper in Sec. III, the analysis of the model is presented in Sec. IV, where we calculate its MF phase diagram and discuss the condensate dynamics. Predictions derived from our MF analysis are shown in Sec. V to agree qualitatively, and in some instances also quantitatively, with with results of numerical simulations. Sec. VI summarizes the conclusions of our analysis. Some of the more technical aspects of the analysis and numerics are presented in the Appendices.

II. DESCRIPTION OF THE MODEL AND MAPPING TO A ZRP

The AEP dynamics can be represented in two seemingly different ways which are in fact equivalent. One representation is as a variant of the TASEP and the other as a variant of the ZRP. The equivalence of these two descriptions corresponds to the well known mapping of exclusion processes to ZRPs [1]. In this section we present the definition of the model in these two different pictures, and then discuss how the mapping from one picture into the other is achieved. Below we refer to the model in the exclusion process picture simply as the AEP, while we call the other "the ZRP picture". Note that we use below the term "ZRP picture" to highlight similarities to the ZRP, even though the model is not strictly "zero range" in nature.

The original definition of the AEP in Ref. [39] is as an exclusion process similar to the TASEP. In this model, N particles are distributed among $L_{\rm AEP}$ sites of a one-dimensional lattice (we add the subscript AEP for later convenience). The particles have an exclusion interaction which does not allow two or more particles to reside on the same site, and therefore each site is either empty or occupied by a single particle. The dynamics of the model, illustrated in Fig. 1a, proceeds as follows: a particle at site i may hop to $i+1$ with rate (i.e., probability per unit time) 1, provided site $i+1$ is empty (here $i = 1, \ldots, L_{\rm AEP}$ is an arbitrary site). If an advancing particle joins an existing cluster of k particles, i.e. if sites $i+2, \ldots, i+k+1$ are occupied but $i+k+2$ is empty, it may facilitate a (simultaneous) hop of the particle at the other end of the cluster from site $i+k+1$ to $i+k+2$. The second, facilitated, hop occurs if and only if the cluster is of length $1 \le k \le \ell_{\rm max}$, where $\ell_{\rm max} \le L$ is a parameter of the model. The model thus has three parameters $(L_{\rm AEP}, N, \ell_{\rm max})$. In the current work we focus on the thermodynamic limit in which $L_{\rm AEP}, N \to \infty$ while their ratio, the particle density $\rho_{\rm AEP} \equiv N/L_{\rm AEP}$, remains fixed. The particle current of this model is always larger than the current of the corresponding TASEP (which is the same model with no facilitated hops), and for this reason it was called an accelerated exclusion process in Ref. [39].

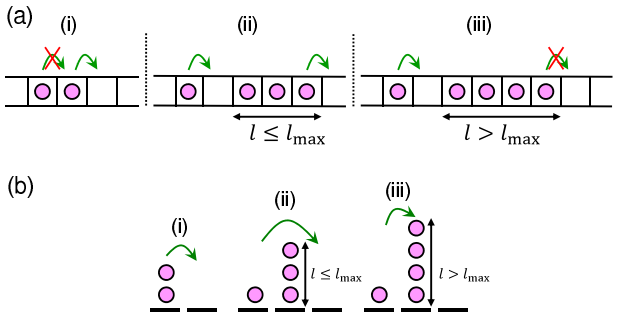

FIG. 1. (a) A schematic representation of the dynamics of the AEP for $l_{\rm max} = 3$. (i) Particles hop in a totally asymmetric fashion subject to exclusion interactions. (ii) When a particle joins a cluster of length $l \le l_{\rm max}$, it triggers an additional hop at the front of the cluster (note that only one hop is triggered, i.e., no "avalanches" develop). (iii) A second hopping is *not* triggered, however, when the cluster is of size $l > l_{\rm max}$. (b) The same model, mapped to a ZRP-like picture: each vacancy in the exclusion process is mapped to a ZRP site, and the size of the cluster to the right of the vacancy is mapped to the occupation of the ZRP site.

We now describe the model in the ZRP picture. In this picture, there are $L_{\rm ZRP}$ sites, each occupied by a fluctuating number of particles n_i where the index $i = 1, \ldots, L_{\rm ZRP}$ is again used to denote sites in the lattice. Unlike the TASEP picture, in the ZRP picture there is no restriction on the number of particles per site, and therefore $n_i \ge 0$ can attain any positive integer value. The dynamics proceeds with particles hopping stochastically among sites as follows. An occupied site i ejects a particle with rate 1. The particle then hops in a totally asymmetric fashion: if site $i+1$ is empty, or if it has more than $\ell_{\rm max}$ particles, the particle moves to $i+1$. Otherwise, i.e. if $1 \le n_{i+1} \le \ell_{\rm max}$, the particle advances another site and lands at site $i+2$. The dynamics can

be summarized as

$$\begin{aligned} \ldots, n_i, n_{i+1}, n_{i+2}, \ldots &\xrightarrow{\mathbb{1}(n_i \geq 1)} \ldots, n_i - 1, n_{i+1} + 1, n_{i+2}, \ldots \quad \text{if } n_{i+1} = 0 \text{ or } n_{i+1} > \ell_{\max} \\ \ldots, n_i, n_{i+1}, n_{i+2}, \ldots &\xrightarrow{\mathbb{1}(n_i \geq 1)} \ldots, n_i - 1, n_{i+1}, n_{i+2} + 1, \ldots \quad \text{if } 1 \leq n_{i+1} \leq \ell_{\max}, \end{aligned} \tag{1}$$

(see also Fig. 1b) where $\mathbb{1}$(condition) equals one if the condition is met and zero otherwise. This dynamics conserves the total number of particles, $N \equiv \sum_i n_i$. Once again, the model has three parameters, which in the thermodynamic limit of $L_{\rm ZRP}, N \to \infty$ with a constant ratio are reduced to the density $\rho_{\rm ZRP} \equiv N/L_{\rm ZRP}$ and $\ell_{\max}$.

The ZRP picture is obtained from the AEP by focusing on the dynamics of clusters rather than the occupation of sites. Each configuration of an AEP with $L_{\rm AEP}$ site, N particles, and $H \equiv L_{\rm AEP} - N$ holes (i.e., unoccupied sites) can be mapped to a ZRP configuration with $L_{\rm ZRP} = H$ sites and N particles as follows: each hole in the AEP is mapped to a site in the ZRP, and the size of the cluster to the right of the hole (i.e., the number of particles between this hole and the next hole) is mapped to the occupation of the corresponding ZRP site. This mapping is illustrated in Fig. 1. It is straightforward to verify that under this mapping, the dynamics of the AEP is exactly mapped to the ZRP picture dynamics defined above.

Since the number of sites in the AEP and the corresponding ZRP are not the same, the density of particles in the two also differ. The density in one picture can be translated to that of the other according to the relations

$$\rho_{\rm ZRP} = \frac{\rho_{\rm AEP}}{(1-\rho_{\rm AEP})} \qquad \text{and} \qquad \rho_{\rm AEP} = \frac{\rho_{\rm ZRP}}{(1+\rho_{\rm ZRP})}. \tag{2}$$

Similar equations relate the particle currents $J_{\rm ZRP}$ and $J_{\rm AEP}$ in the two systems. In both systems, the current is defined as the total number of sites traversed by hopping particles per unit time divided by the respective system size. Therefore,

$$J_{\rm ZRP} = (1+\rho_{\rm ZRP}) J_{\rm AEP} \quad \text{and} \quad J_{\rm AEP} = (1-\rho_{\rm AEP}) J_{\rm ZRP}. \tag{3}$$

Working in the ZRP picture is more convenient for the purpose of studying condensation in the model. Therefore, in the rest of the paper we concentrate on the ZRP picture and only occasionally translate the results to the exclusion process picture. To simplify notation, in what follows we drop the subscript ZRP and denote $L \equiv L_{\rm ZRP}$, $\rho \equiv \rho_{\rm ZRP}$ and $J \equiv J_{\rm ZRP}$.

III. SUMMARY OF MAIN RESULTS

The AEP was studied numerically in Ref. [39], where several interesting phenomena were found. The most striking result is that for a finite system of $L_{\rm AEP} = 1000$ and several values of $\ell_{\max}$ that range from 10 to 500, there is an apparent transition from a disordered phase at low densities to a condensed phase at high densities. The disordered phase is homogeneous, while in the condensed phase there is a cluster of particles of macroscopic size, consisting of a significant fraction of all particles. The transition is also visible in the current-density relation: in the disordered phase, the current changes nonlinearly with the density, while the condensed phase is characterized by a current $J_{\rm AEP} = 1 - \rho_{\rm AEP}$, which corresponds to $J_{\rm ZRP} = 1$.

Recently, a combination of a MF analysis, exact results, and numerics, was used in Ref. [40] to clarify some of the earlier numerical findings. In particular, the model was analyzed in the homogeneous phase, and also in the special limit of $N \to \infty$ with $L_{\rm ZRP}$ fixed (in the TASEP picture this corresponds to a fixed number of holes). However, several questions that arise naturally from the numerical results remain unanswered. Is there a true phase transition in the thermodynamic limit of the model? What is the order of the phase transition? Can one calculate the phase diagram and explain the simple form of the current in the condensed phase? In the present paper, we seek solutions to these questions within a MF approximation. The results of our analysis are as follows.

1. The mean-field approximation suggests that a true condensation phase transition occurs in the thermodynamic limit when $\ell_{\max}$ diverges with L at least logarithmically, i.e., $\ell_{\max} > C \log L$, for large enough constant C. If $\ell_{\max}$ is kept constant in the limit of $L, N \to \infty$, no phase transition occurs.

2. The transition is continuous when $C \log L < \ell_{\max} \ll L$. The critical density (in the ZRP picture) is $\rho_c = 1$, in agreement with the numerics of Ref. [39]. The current in the critical phase (in the ZRP picture) is $J_c = 1$. As in the ZRP, this current is independent of the density. This explains why holes have a unit velocity in the condensed phase, as found in Ref. [39].

3. The transition becomes discontinuous when $\ell_{\max}$ scales linearly with L, i.e, when $\ell_{\max} = aL$ where a is a constant. The density at the transition point can be obtained within the mean-field approximation by calculating the large deviation function for

the size of the condensate. The transition density satisfies $\rho_{\rm trans}(a) > 1$. The mean-field picture suggests that close to the transition there are metastability and hysteresis effects, which might explain the large fluctuations measured numerically in Ref. [39].

4. In the condensed phase, the condensate drifts by skipping every other site (i.e., it drifts from site 1 to 3 to 5, etc.). This drift is similar to that found recently in Ref. [29]. The drift velocity decays algebraically or faster with the system size (depending on the scaling of $\ell_{\max}$ with L), and the condensate is typically supported on a single site.

5. Although the MF description is usually expected to be only qualitatively correct, some of our MF predictions, including the phase diagram, quantitatively match numerical results to a high accuracy. It is not yet known whether the mean-field approximation indeed yields the exact phase diagram of the model, and if so, why.

IV. CONDENSATION TRANSITION IN THE AEP

In this section, we use the mean-field (MF) approximation of Ref. [29] to analyze the AEP condensation transition. In MF analyses of models such as the AEP, one usually assumes that the occupations of different sites are independent and identically distributed. In the MF picture we employ here, the occupations of different sites are assumed to be independent in the steady-state, but not necessarily identically distributed. In particular, in the condensed phase, where the condensate spontaneously breaks the translational symmetry of the model, the occupation probability of a site is allowed to depend on its distance from the condensate. Indeed, due to spatial correlations, the *true* marginal occupation probability of a site is expected to vary with the distance from the condensate. Thus, the non-homogeneous MF ansatz which we consider effectively captures some of the effects of correlations between sites, even though sites are ultimately assumed to be independent. Allowing the steady state distribution to be inhomogeneous (even though the dynamics is translationally invariant) is the main technical novelty of our approach.

Mathematically stated, the MF assumption postulates that the stationary distribution has a product form

$$P_\rho^{gc}(n_1,\ldots,n_L) = \prod_{i=1}^{L} P_i(n_i|\rho), \tag{4}$$

where $P_i(n|\rho)$ denotes the probability that, within this mean-field approach, site i has exactly n particles in the steady state. The single site distributions $P_i(n|\rho)$ depend on the density ρ via the requirement that the mean total number of particles satisfies

$$\sum_{i=1}^{L}\sum_{n_i=0}^{\infty} n_i P_i(n_i|\rho) = L\rho. \tag{5}$$

The ansatz (4) is "grand-canonical" in nature, in the sense that the total number of particles in the system is allowed to fluctuate around its mean (5). Such an ansatz is expected to be useful for the description of typical fluctuations in the steady state (and possibly also in metastable states). However, one cannot hope that it successfully describes, for example, the probability that a single site accommodates all N particles. More generally, the ansatz must be adjusted in any event where the occupations of some sites are so large that, due to the constraint on the total particle number, a macroscopic fraction of all other sites is forced to be in an atypical state. In order to describe such situations, one should consider a "canonical" distribution, where the total number of particles is constrained. To simplify the calculation, we instead propose a "hybrid" ansatz, in which sites are split into two groups — macroscopically occupied sites (the condensate), and the rest (the fluid background). The distribution of the fluid is still taken as to be factorized, but its mean occupation depends on the occupation of the condensate sites. For a configuration with k condensate sites with occupations $n_{j_i} = m_i L$ (for $i = 1,\ldots,k$), this ansatz may be written as

$$P_\rho^{c}(n_1,\ldots,n_L) = P_{\max}^{(k)}(\mathbf{m}) \prod_{i} P_i\Big(n_i\Big|\rho - \sum m_i\Big), \tag{6}$$

where $P_{\max}^{(k)}(\mathbf{m})$ is the probability that the k most occupied sites have occupations $\mathbf{m}L \equiv (m_1 L,\ldots,m_k L)$, and the product runs over all sites other than $j_1,\ldots,j_k$. This ansatz is not adequate for the description of the most general situations, but it shall suffice for the calculation of the AEP phase diagram. Abusing the terminology somewhat, we call this ansatz below the canonical ansatz. Note that $P_{\max}^{(k)}$ may depend not only on the occupations of the highly occupied sites, but also on their locations. We suppress this dependence in the notation to avoid clutter. In addition, in what follows, the dependence of P_i on ρ shall also be suppressed, i.e., we shall denote $P_i(n_i) \equiv P_i(n_i|\rho)$.

For the calculation of the phase diagram, the grand-canonical ansatz (4) suffices if a condensate can be created without macroscopically affecting all other sites. This happens when $\ell_{\max} \ll L$, as the occupation of any site may in this case reach $\ell_{\max}$ without noticeably affecting the occupations of other sites. However, when $\ell_{\max} = aL$ (where a is a finite constant), a finite fraction of all particles in the system must be located in a single site if its occupation is to reach $\ell_{\max}$, and the state of *all* other sites is influenced. Therefore, the canonical ansatz (6) must be employed to analyze this case. We show below that in the first case ($\ell_{\max} \ll L$), the condensation transition is continuous, while it becomes discontinuous

in the second case ($\ell_{\max} = aL$). The inadequacy of the grand-canonical ansatz in the latter case is a manifestation of an inequivalence of the two ensembles. This is similar to the behavior of equilibrium systems with long-range interactions, where first order phase transitions may lead to inequivalence of ensembles [43, 44]. A condensation transition with very a similar phenomenology, and indeed a similar mathematical description, has been studied in Refs. [14, 20, 35, 45] in a ZRP with with rates that depend on the system size L. The methods of analysis presented in these works will prove useful in what follows.

We begin the calculation by considering, in Sec. IV A, the case of $\ell_{\max} \ll L$, where the phase diagram can be calculated using the grand-canonical ansatz (4). The grand-canonical calculation is simpler than the canonical one, as sites are completely independent of each other according to the assumption (4). Therefore, the description of the MF procedure is more transparent in the grand-canonical ensemble. We then move on to the case of $\ell_{\max} = aL$, where ensembles are inequivalent. The canonical calculation in this case is presented in Sec. IV B.

A. Grand-canonical calculation, $\ell_{\max} \ll L$

Assume that the steady-state distribution has the form (4). Our goal is to find the single-site marginals $P_i(n)$. Before writing down the master equation that these marginals satisfy, we define two auxiliary quantities that simplify subsequent notation: by q_i we denote the mean influx of particles into site i conditioned on its occupation satisfying $1 \le n_i \le \ell_{\max}$. Similarly, we write Q_i to denote the mean influx conditioned on $n_i = 0$ or $n_i > \ell_{\max}$. Within the MF approximation, these are equal to

$$\begin{aligned} q_i &= \Big(\sum_{k=1}^{\ell_{\max}} P_{i-1}(k)\Big)\big(1 - P_{i-2}(0)\big) \\ Q_i &= q_i + \big(1 - P_{i-1}(0)\big) \ge q_i. \end{aligned} \tag{7}$$

The first line states that when $1 \le n_i \le \ell_{\max}$, the only particles that are added to site i are those that leave site $i-2$ (these hop with rate 1 whenever site $i-2$ is not empty), and do not stay at site $i-1$ (i.e., $1 \le n_{i-1} \le \ell_{\max}$). The second line states that when $n_i = 0$ or $n_i > \ell_{\max}$, the incoming current into site i is higher because it also includes all particles which depart from of site $i-1$.

Using this notation, the master equation reads

$$\begin{aligned} \dot{P}_i(0) &= P_i(1) - P_i(0)Q_i \\ \dot{P}_i(1) &= P_i(2) + P_i(0)Q_i - P_i(1)[1+q_i] \\ \dot{P}_i(n) &= P_i(n+1) + P_i(n-1)\mathcal{Q}_i(n-1) \\ &\quad - P_i(n)[1+\mathcal{Q}_i(n)], \end{aligned} \tag{8}$$

where

$$\mathcal{Q}_i(n) \equiv \begin{cases} q_i & \text{if } 1 \le n \le \ell_{\max} \\ Q_i & \text{if } n = 0 \text{ or } n \ge \ell_{\max}+1 \end{cases}. \tag{9}$$

In the steady state the left hand sides of Eqs. (8) vanish and they can be recursively solved, yielding

$$P_i(n) = P_i(0) \begin{cases} Q_i q_i^{n-1} & \text{if } 1 \le n \le \ell_{\max}+1 \\ Q_i^{n-\ell_{\max}} q_i^{\ell_{\max}} & \text{if } n \ge \ell_{\max}+1 \end{cases}. \tag{10}$$

Assuming that $Q_i < 1$ (an assumption that will be examined below), the normalization condition $\sum_n P(n) = 1$ yields

$$P_i(0) = \frac{(1-q_i)(1-Q_i)}{1 - q_i - Q_i(Q_i - q_i)(1 - q_i^{\ell_{\max}})} \simeq \frac{1-q_i}{1+Q_i-q_i}, \tag{11}$$

where the last approximate equality becomes exact in the limit $\ell_{\max} \to \infty$. Similarly, the mean occupation of site i is, when $\ell_{\max} \to \infty$,

$$\rho_i \equiv \sum_n n P_i(n) \simeq \frac{Q_i}{(1-q_i)(1+Q_i-q_i)}. \tag{12}$$

The distribution (10) is normalizable only as long as q_i and Q_i are both less than 1. If Q_i (the larger of the two) is found to be 1 or more, the above analysis is inconsistent. Physically, such an inconsistency means that site i tends to accumulate an ever-increasing number of particles, signalling that a condensate forms on site i. If $Q_i < 1$ for all densities ρ, then there is no condensation transition in the model. Below we show that this is not the case, and that a condensation transition occurs at a critical density ρ_c at which $Q(\rho_c) = 1$. We proceed by analyzing separately the subcritical phase, in which the system is homogeneous, and the supercritical phase in which the condensate breaks translational invariance.

1. *The homogeneous phase*

In the homogeneous phase, P_i, q_i and Q_i are site independent, and therefore the subscript i may be dropped. From equations (7) and (11) it is found that when $\ell_{\max} \to \infty$

$$Q = q + \sqrt{q} \quad \text{or equivalently} \quad q = \frac{1}{2}\big(1 + 2Q - \sqrt{1+4Q}\big). \tag{13}$$

Substituting this relation in Eq. (12) yields

$$Q = \frac{1 - \rho + 2\rho^2 - (1-\rho)\sqrt{1+4\rho^2}}{2\rho^2}. \tag{14}$$

It is seen that $Q(\rho \to 1) = 1$, implying that the calculation breaks down at a critical density

$$\rho_c \equiv 1. \tag{15}$$

This breakdown signals the occurrence of a condensation transition at ρ_c (remember that this is true only when the grand-canonical ensemble is equivalent to the canonical ensemble, i.e., when $1 \ll \ell_{\max} \ll L$. As discussed below, when $\ell_{\max}$ scales linearly with L the condensation transition occurs at a density $\rho_{\rm trans} > \rho_c$). In the exclusion process picture, the corresponding critical density is $\rho_{{\rm AEP},c} = 1/2$ [see Eq. (2)], which is in agreement with the findings of Ref. [39].

2. The supercritical phase

The mean-field analysis of the supercritical phase begins by assuming that there is a "supercritical site" whose occupation is macroscopic. The following analysis is thus valid as long as this site remains macroscopically occupied. On very large timescales (which will be determined below), the condensate migrates to other sites. Our analysis relies on the wide separation between the timescale of the microscopic dynamics and the macroscopic timescale of condensate motion.

Assume that a condensate is located on site 1, i.e., $n_1 \approx \infty$. This information can be used in Eq. (7) to find that $q_2 = 0$ and $Q_2 = 1$, and thus from (10) and (11) we obtain $P_2(0) = P_2(1) = 1/2$, and $P_2(n \geq 2) = 0$. We may now repeat the procedure to calculate $P_3(n)$ [and iteratively $P_i(n)$ for any i]. We thus find $q_3 = 1/2$ and $Q_3 = 1$. This value of Q implies that $P_3(n)$ is not normalizable, i.e., site 3 is "critical': once n_3 exceeds the value $\ell_{\max}$, the incoming current into this site exactly equals the outgoing current, and n_3 might increase and eventually take over the condensate. However, in the condensed phase the time it takes n_3 to reach the value $\ell_{\max}$ is very long — this is in fact a requirement for the condensed phase to exist, as we discuss below. Therefore, for long periods of time the system is in a metastable state in which n_3 fluctuates around 0. We analyze the two cases $n_3 = O(1)$ and $n_3 > \ell_{\max}$ separately.

We begin by examining the long-lived metastable state in which n_3 remains finite. In this metastable state, n_3 performs a random walk biased towards $n_3 = 0$ with a reflecting boundary condition at the origin. This random walk has an absorbing wall at $n_3 = \ell_{\max}+1$. Conditioned on the walk not reaching this absorbing wall, we find from Eqs. (10) and (11) that (for $\ell_{\max} \gg 1$) $P_3(0) \simeq 1/3$ and $P_3(n) \simeq 2^{-(n-1)}/3$ for $n \geq 1$. Moving to site 4 we find $q_4 = 1/3$ and $Q_4 = 1$, i.e., site 4 is also critical. Once again, there is a long-lived metastable state in which n_4 is finite, and eventually, when n_4 reaches $\ell_{\max}$, it might increase until it takes over and becomes the new condensate. This picture continues at all sites, and as before we first examine the metastable state in which all sites have finite occupations, $n_i \leq \ell_{\max}$. Continuing the procedure iteratively, we show in Appendix A that $Q_i = 1$ for all $i \geq 2$, $q_i = P_{i-1}(0)$, and $P_i(0) = F_{i-1}/F_{i+1}$ where F_i is the i'th Fibonacci number. Therefore, q_i and $P_i(0)$ converge exponentially with i to $q_\infty \equiv (3-\sqrt{5})/2 \approx 0.38$.

We now examine what happens once a site $2 \leq i \leq L$ reaches $n_i = \ell_{\max}+1$. As long as n_i remains larger than $\ell_{\max}+1$, it performs an unbiased random walk. If it reaches $\ell_{\max}+1$ the random walk becomes biased again towards $n_i = 0$, and the occupation rapidly decreases to its metastable, nearly-empty state. On the other hand, if it reaches $n_i \approx N_{\rm cond} - \ell_{\max}$ (where $N_{\rm cond}$ is the typical number of particles in the condensate) the old condensate becomes depleted and site i takes over and becomes the new condensate. There is of course a possibility that while $\ell_{\max} < n_i < N_{\rm cond} - \ell_{\max}$, another site (or sites) reaches $\ell_{\max}+1$, leading to a situation with three (or more) highly occupied site. If this event is quite probable, the system typically does not have just a single condensate but many highly occupied sites (possibly a finite density of them), and therefore the system will not be in a truly condensed state.

In order to ensure that typically there is only one highly occupied site at a time, and, on rare occasions, no more than two such sites, one must choose $\ell_{\max}$ to be large enough so that the time $T_{\ell_{\max}}$ that it takes until some site reaches $\ell_{\max}$ is much larger than the time $T_{\rm takeover}$ that passes before a highly occupied site takes over the condensate. Since $\ell_{\max} \ll N_{\rm cond} = O(L)$, the latter scales as $T_{\rm takeover} = O(N_{\rm cond}^2) = O(L^2)$ (this is the well-known gambler's ruin problem for an unbiased random walk). On the other hand, $T_{\ell_{\max}}$ scales as

$$T_{\ell_{\max}} = O\Big(\big[\sum_i q_i^{\ell_{\max}}\big]^{-1}\Big) \approx O\Big(\min\big(q_3^{-\ell_{\max}}, q_\infty^{-\ell_{\max}}/L\big)\Big). \tag{16}$$

The first of the two terms on the right hand site of (16) corresponds to the time it takes site 3 to reach $\ell_{\max}$ particles (the probability of site 3 to reach $\ell_{\max}$ is higher than that of any other site because $q_3 > q_i$ for all sites i), and the second corresponds to a distant site (with $q_i \approx q_\infty$) reaching $\ell_{\max}$ (although this probability is smaller than that of site 3, there are $O(L)$ such sites, increasing the probability that one of them reaches $\ell_{\max}$). The condition $T_{\ell_{\max}} \gg T_{\rm takeover}$ then implies that

$$\ell_{\max} \gg \frac{3}{-\log q_\infty}\,\log L \approx 3.12\,\log L \tag{17}$$

must hold in order for the system to have a single condensate. This means that a true condensation transition takes place only when $\ell_{\max}$ increases logarithmically (where the logarithm has a large enough prefactor) or faster with the system size. The same criterion for condensation was suggested in a similar model in Ref. [14]

3. Dynamics of the condensate

We now discuss the dynamics of the condensate. We begin by noting that when $\log L \lesssim \ell_{\max} \ll L$, it is highly improbable for an AEP with a supercritical density to be (momentarily) in a homogeneous disordered state, i.e., where no occupation exceeds $\ell_{\max}$. This fact can once

again be understood dynamically: the condensate must lose $O(L)$ particles without a new condensate forming in order for the system to reach such a disordered state. The typical timescale in which this process occurs is exponentially large: e^{cL} for some constant c, essentially since this process necessitates that *all* other (independent) sites are to be atypically occupied (see below in Sec. IV B). On the other hand, if the system is in a disordered state, it takes a time of order $O(q_i^{-\ell_{\max}}) \ll e^{cL}$ for a site to reach $\ell_{\max}$ and a condensate to form. Therefore, the fraction of time the system spends in a disordered state is negligible in the thermodynamic limit.

Thus, the dynamics of the condensate is dominated by events where an additional condensate forms on another site, eventually taking over the old one. Where and when does this new condensate form? First, consider the case that $\ell_{\max} = A \log L$ with A large enough so that typically there is indeed a single condensate. As discussed above, from time to time a fluctuation may cause another site to reach $\ell_{\max}$ and (with some probability) to take over the condensate. What is the most probable location of the new condensate? To answer this question, compare the time it takes site 3 to reach $\ell_{\max}$, which is of order $O(L^{-A \log q_3})$, with the time it takes a distant site to reach $\ell_{\max}$, which is of order $O(L^{-A \log q_\infty - 1})$ (remember that there are $O(L)$ such distant sites). Comparing these, we find that when $A > [\log(q_3/q_\infty)]^{-1} \approx 3.71$ the new condensate forms most frequently on site 3, i.e., two sites downstream from the current condensate. In this case, the condensate performs a drift motion, skipping every other site. In the thermodynamic limit, however, the drift velocity of the condensate decreases to zero algebraically with the system size, as $L^{-A \log 2}$.

When $\log L \ll \ell_{\max} \ll L$ (e.g., $\ell_{\max} \sim \sqrt{L}$), the argument of the previous paragraph shows that a condensate at site i always relocates to site $i+2$, and the resulting drift velocity is of order $2^{-\ell_{\max}}$. This velocity decreases with the system size faster than algebraically but slower than exponentially (e.g., as a stretched exponential when $\ell_{\max} \sim \sqrt{L}$).

B. Canonical calculation, $\ell_{\max} = aL$

As discussed above, when $\ell_{\max} = aL$ the analysis must proceed in the canonical ensemble. We now show that in this case the condensation phase transition is of first, rather than second, order. Thus, the canonical and grand-canonical ensembles are inequivalent. Our analysis of this case follows the ideas of Ref. [45]: to find the density at which there is a phase transition, we shall calculate the occupation probability of the most occupied site, or more precisely, the large-deviation function (LDF) for this occupation [46]. This LDF is found by examining the dynamics of the condensate occupation. The condensate LDF plays a role similar to that of an equilibrium free energy, and thus once it is found a Landau-theory-type analysis yields the phase diagram of the model.

1. Calculation of the condensate LDF

The calculation of the LDF proceeds in three steps: (i) we express the LDF in terms of the currents entering and leaving the condensate; (ii) we express these currents as a function of the density of the background fluid; and (iii) we discuss how the background density depends on the occupation of the condensate.

Step (i). Assume that the condensate has $n_{\max} = mL$ particles (here we use the word condensate to mean the most occupied site). Denote by $J_{\rm in}(m)$ the mean momentary current flowing into the condensate conditioned on this occupation, and similarly by $J_{\rm out}(m)$ the mean current flowing out of the condensate. Within the canonical MF ansatz (6), these currents might depend on m through the constraint on the total number of particles, but there are no further correlations between the condensate and the rest of the system. In other words, the rest of the system may determine the functions $J_{\rm in}(m)$ and $J_{\rm out}(m)$, but otherwise one may consider the dynamics of the condensate separately from that of the rest of the system. Denoting $P_{\max}(n) \equiv P(n_{\max} = n)$, the master equation for the condensate occupation is thus

$$\begin{aligned}\dot{P}_{\max}(mL) = {} & P_{\max}(mL-1) J_{\rm in}(m - L^{-1}) \\ & + P_{\max}(mL+1) J_{\rm out}(m + L^{-1}) \\ & - P_{\max}(mL) \big[J_{\rm in}(m) + J_{\rm out}(m) \big]. \end{aligned} \tag{18}$$

Equating the left-hand side of (18) to zero, and substituting the LDF ansatz

$$P_{\max}(mL) \sim e^{-L I_\rho(m)} \tag{19}$$

yields to leading order in L

$$\begin{aligned} 0 & \sim e^{I'_\rho(m)} J_{\rm in}(m) + e^{-I'_\rho(m)} J_{\rm out}(m) - [J_{\rm in}(m) + J_{\rm out}(m)] \\ & = \big(1 - e^{I'_\rho(m)}\big) \big(e^{-I'_\rho(m)} J_{\rm out}(m) - J_{\rm in}(m)\big) \end{aligned} \tag{20}$$

(this is similar to the WKB approximation in quantum mechanics). Since the first brackets on the right-hand side cannot be identically zero, we obtain

$$I_\rho(m) = -\int^m \log \frac{J_{\rm in}(m')}{J_{\rm out}(m')}\, dm' + C, \tag{21}$$

where C is an integration constant which can be obtained by the normalization requirement $\min I_\rho(m) = 0$.

Step (ii). The goal now is to find the functions $J_{\rm in}(m)$ and $J_{\rm out}(m)$. The latter is simply $J_{\rm out}(m) = 1$, as the departure of particles from the condensate is independent of its size and of the rest of the system. To find the former, we assume that at any value of condensate occupation m, the background fluid can be described by Eqs. (10)–(12). This would be the case, for instance, if the relaxation timescale of the background fluid is much shorter than the timescale in which the condensate density $m = n_{\max}/L$ changes. Although we cannot justify

this assumption a priori, we will see below that predictions of the ensuing calculation are very close to results measured in numerical simulations.

We continue by obtaining from Eqs. (7) and (11) a recursion relation for $P_i(0)$:

$$P_{i+1}(0) = \frac{P_i(0) + P_{i-1}(0) - P_i(0)P_{i-1}(0)}{2 - P_i(0)}. \qquad (22)$$

This recursion relation is analyzed in Appendix B, where it is shown that all values $0 < P_\infty(0) < 1$ are fixed points of this map, and furthermore the map is exponentially contracting towards these fixed points. Thus, the bulk of the fluid background is effectively described by the appropriate fixed point, with deviations only in a finite boundary layer near the condensate. The fixed point is dictated by the condition $\rho_\infty = \rho_{\rm bg}(m)$, where [from Eqs. (7), (11) and (12)]

$$P_\infty(0) = \frac{1 + 2\rho_\infty - \sqrt{1 + 4\rho_\infty^2}}{2\rho_\infty}. \qquad (23)$$

The density of particles in the background fluid, $\rho_{\rm bg}(m)$, will be discussed in step (iii).

The condensate is located in site 1, which is also site $L+1$ (due to the periodic boundary conditions). Therefore, the current into the condensate is $q_{L+1} \simeq q_\infty$ when $n_{\max} < \ell_{\max}$, i.e., when $m < a$, and it is $Q_{L+1} \simeq Q_\infty$ when $m > a$. Using Eq. (7), we finally arrive at

$$J_{\rm in}(m) = 1 - \frac{S-1}{2\rho_{\rm bg}^2} \times \begin{cases} 1 & \text{if } m < a \\ 1 - \rho_{\rm bg} & \text{if } m > a \end{cases}, \qquad (24)$$

where $S = \sqrt{1 + 4\rho_{\rm bg}^2}$, and $\rho_{\rm bg} = \rho_{\rm bg}(m)$ is the density of the background fluid.

The functions $J_{\rm in}(m)$ and $J_{\rm out}(m)$ are plotted in Fig. 2 for $\rho = 2 > \rho_c$, assuming (as we shall, see next step) that $\rho_{\rm bg}(m) = \rho - m$. We see that there is one point where $J_{\rm in}(m) = J_{\rm out}(m)$: at $m = \rho - 1$. At this point, the current entering the condensate equals that leaving it, and thus the condensate occupation is fixed. Furthermore, this fixed point is locally stable: if m decreases the incoming current increases and vice versa. Note, however, that this fixed point exists only if $\rho - 1 > a$ [as the jump in the curve of $J_{\rm in}(m)$ occurs at $m = a$]. In addition, $m = 0$ is always a locally stable fixed point, due to the boundary condition $J_{\rm out}(0) = 0$ [47]. Thus we see that when $\rho < 1 + a$ the only stable solution is a disordered phase with no condensate ($m = 0$), while when $\rho > 1 + a$ there are two locally stable states: a disordered phase, and a condensed phase where a condensate of size $m = \rho - 1$ coexists with a background of density $\rho_{\rm bg} = 1 = \rho_c$. To find out which of these dominates in the thermodynamics limit one must carry out the integration of Eq. (21).

Step (iii). The remaining task is to find the function $\rho_{\rm bg}(m)$. Naively, one might assume that all particles which are not in the condensate are in the background, i.e., $\rho_{\rm bg}(m) = \rho - m$. However, when the condensate occupation m becomes much lower than its typical value,

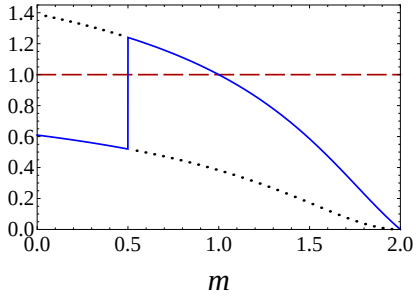

FIG. 2. The incoming current into the condensate $J_{\rm in}(m)$ (solid line) and the outflowing current $J_{\rm out}(m)$ (dashed line) as a function of the condensate fraction m, for $\rho = 2$ and $a = 0.5$. The two branches of the function $J_{\rm in}(m)$ [Eq. (24)] are indicated by dotted lines.

the excess particles (or at least some of them) might not accumulate in the background fluid, but rather in a single site (or a few sites), thus forming new condensates. Denote by $m_2 \le m$ the fraction of particles in the second most occupied site. The occupation probability of the two most occupied sites again has a large deviations form

$$P^{(2)}_{\max}(mL, m_2 L) \sim e^{-L I^{(2)}_\rho(m, m_2)}, \qquad (25)$$

and the condensate LDF is given by contraction:

$$I_\rho(m) = \min_{m_2} I^{(2)}_\rho(m, m_2) = I^{(2)}_\rho\big(m, m_2(m)\big), \qquad (26)$$

where $m_2(m)$ is the value of m_2 which achieves the minimum of $I^{(2)}_\rho$ for a given value of m. Solving this minimization problem is a difficult task — instead of solving the ODE (20) one must solve a PDE which is a two-dimensional version of this equation, see Appendix C. Furthermore, some values of m and m_2 are most probably achieved by other macroscopically occupied sites forming, with occupations $m_3 L, m_4 L$, etc.. To study these, one must analyze even higher dimensional LDFs of the form $I^{(k)}_\rho(m, m_2, m_3, \ldots, m_k)$. In light of this discussion, it is seen that the background density is $\rho_{\rm bg}(m) = \rho - m - m_2(m) - m_3(m) - \ldots$.

Here we shall not go through this higher dimensional analysis to compute the exact form of $I_\rho(m)$. Instead, we first substitute

$$\rho_{\rm bg}(m) = \rho - m \qquad (27)$$

and compute the LDF $\tilde{I}_\rho(m)$ when the system is constrained to have no more than one condensate site. This LDF is an upper bound on the true, unconstrained LDF:

$$\tilde{I}_\rho(m) = I^{(2)}_\rho(m, 0) \ge I_\rho(m) \qquad (28)$$

[see (26) and Appendix C]. In Sec. IV B 3 below we shall show that for a large range of m values the two are equal, $\tilde{I}_\rho(m) = I_\rho(m)$. In particular, we argue that $\tilde{I}_\rho(m)$ suffices for the calculation of the phase diagram.

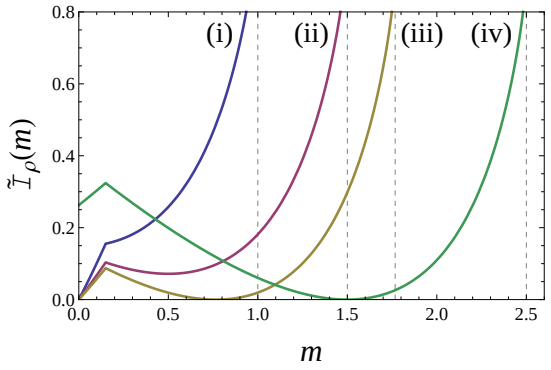

FIG. 3. The large-deviation function $\tilde{I}_\rho(m)$ of the occupation fraction of the most occupied site for $a = 0.15$ and different densities: (i) $\rho = 1$, (ii) $\rho = 1.5$, (iii) $\rho = \rho_{\rm trans} \approx 1.77$, (iv) $\rho = 2.5$. The first order transition is clearly seen: at densities below $\rho_{\rm trans}$ the global minimum is at $m = 0$, while above $\rho_{\rm trans}$ it is at $m = \rho - 1$.

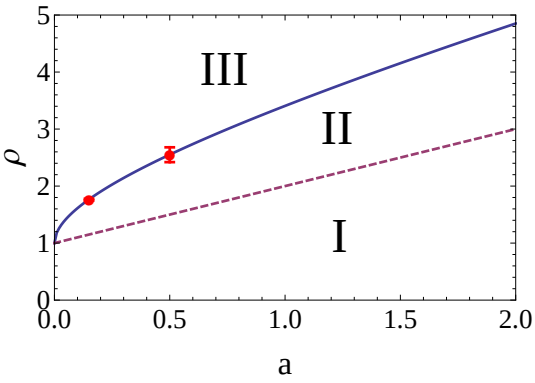

FIG. 4. The mean-field phase diagram. Regions I and II are the disordered fluid phase, and region III is the condensed phase. The solid line marks the first order transition line $\rho_{\rm trans}(a)$, and the dashed line, $\rho = a + 1$, marks the edge of stability of the condensed phase. Accordingly, in region II the condensed phase is metastable, while it is unstable in region I. The two dots with error bars (at $a = 0.15$ and $a = 0.5$) were obtained from simulations of the model, see Sec. V below.

Combining Eqs. (21), (24) and (27) yields the desired (upper bound on the) LDF:

$$\tilde{I}_\rho(m) = \rho_{\rm bg}(m) \log J_{\rm in}(m) + A(m) + C(a,\rho), \qquad (29)$$

where

$$A(m) \equiv \begin{cases} \log(S - 2\rho_{\rm bg}) + c(a,\rho) & \text{if } m < a \\ [3\log(S - 2\rho_{\rm bg}) + 1 + 2\rho_{\rm bg} - S]/4 & \text{if } m > a \end{cases}, \qquad (30)$$

$S = \sqrt{1 + 4\rho_{\rm bg}(m)^2}$ as before, $\rho_{\rm bg} \equiv \rho_{\rm bg}(m)$ is given in (27), and c, C are two integration constants. The value of $c(a,\rho)$ is chosen so that $\tilde{I}_\rho(m)$ is continuous at $m = a$, while $C(a,\rho)$ is chosen to ensure the normalization $\min_m \tilde{I}_\rho(m) = 0$ (the exact expressions for these integration constants are not reproduced here). In Fig. 3, we plot $\tilde{I}_\rho(m)$ for a few values of ρ.

2. *The mean-field phase diagram*

We are at last in a position to analyze the MF phase diagram of the AEP (using the LDF $\tilde{I}_\rho(m)$; we postpone showing that it indeed yields the correct MF phase diagram to the next paragraph). The typical value of m is the one which attains the global minimum of the LDF (29), which we denote by m^*. All other values of m are exponentially unlikely in L. Any local minimum of $\tilde{I}_\rho$ other than m^* is a metastable state. Such metastable states, although unlikely, have a lifetime that grows exponentially with L, as the system must overcome an exponential barrier before the condensate occupation fraction can reach m^*. The local minima are precisely those found above: studying the LDF (29), it is seen that the $m < a$ branch of $\tilde{I}$ is a monotonically increasing function and thus $m = 0$ is always a local minimum, while the $m > a$ branch is a convex function with a minimum at $m = \rho - \rho_c$ [recall that $\rho_c = 1$, see (15)]. The second local minimum exists, of course, only if $\rho > 1 + a$, otherwise this minimum falls outside the domain $m > a$. The thermodynamic transition point $\rho_{\rm trans}$ occurs when these two minima are equal, i.e., it is implicitly given by the equation

$$\tilde{I}_{\rho_{\rm trans}}(0) = \tilde{I}_{\rho_{\rm trans}}(\rho_{\rm trans} - 1). \qquad (31)$$

The resulting phase diagram is presented in Fig. 4. Note that in the limit of $a \to 0$, the first order phase transition becomes a second order one at ρ_c, as discussed above in Sec. IV A.

3. *The condensate LDF with multiple condensates*

We now discuss the condensate occupation LDF $I_\rho(m)$ when there are multiple condensate sites, and argue that the upper bound $\tilde{I}_\rho(m)$ suffices for the calculation of the phase diagram. As explained above, $\tilde{I}_\rho(m)$ is calculated under the assumption (27), i.e., that there is almost surely only one condensate site for any value of m. This assumption is clearly correct when $m < a$, because then all occupations are below $\ell_{\rm max}$ and the balance of incoming and outgoing particle currents drive all sites towards the background density (see Fig. 2). It is thus exponentially unlikely (in L) to have $m_2 > 0$ in this regime. Similarly, Eq. (27) also holds when $m > \rho - 1$, because in this case the background density satisfies $\rho_{\rm bg}(m) \le \rho - m < 1 \equiv \rho_c$, and thus $Q_\infty(m) < 1$ [see Eq. (14)], i.e., the background fluid is subcritical.

When $a < m < \rho - 1$, Eq. (27) leads to $\rho_{\rm bg}(m) > 1$ and thus $Q_\infty > 1$. In this case one might worry that new condensates could form on other sites. However, as explained throughout this section, when $\ell_{\rm max} = aL$ the

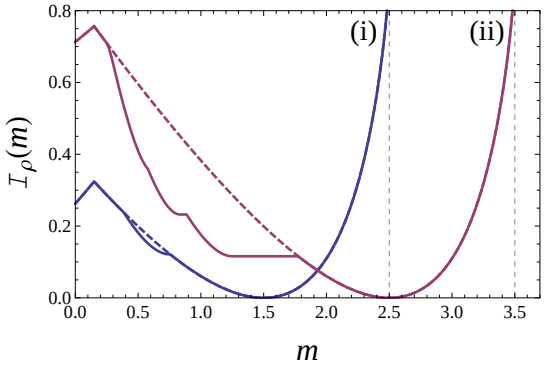

FIG. 5. A schematic illustration of the LDF $I_\rho(m)$ of the condensate occupation fraction (solid line), compared with the upper bound $\tilde{I}_\rho(m)$ (29) (dashed line). The plot is for $a = 0.15$ and densities (i) $\rho = 2.5$, and (ii) $\rho = 3.5$. At high enough densities, more condensates may form as m is conditioned to have increasingly atypical (i.e., lower) values. This is illustrated (schematically) by depicting a second condensate appearing when $\rho = 2.5$, and up to 4 condensates when $\rho = 3.5$. A non-analyticity of $I_\rho(m)$ is manifest at each value of m where a new condensate appears. As explained in the text, $I_\rho(m) = \tilde{I}_\rho(m)$ near both local minima, and thus $\tilde{I}_\rho(m)$ suffices for the calculation of the phase diagram.

condensation transition is first order, and the formation of a condensate does not happen at ρ_c but at a higher transition density. Therefore, a second condensate appears only when $\rho - m > \rho_{\rm trans,2} > 1$ for some transition density $\rho_{\rm trans,2}$. Similarly, a third condensate site appears only when $\rho - m - m_2 > \rho_{\rm trans,3} > 1$ (where m_2 is the fraction of particles in the second condensate site), and so on. For any value of ρ and m, the number of condensate sites that typically appears is finite [45]. A schematic illustration of $I_\rho(m)$ at high values of ρ where multiple condensates may appear is presented in Fig. 5. We conclude that $\tilde{I}_\rho(m) = I_\rho(m)$ around both minima of $\tilde{I}_\rho(m)$ (i.e., around $m = 0$ and $m = \rho - 1$), and thus the transition point calculated in (31) is correct (within the MF approximation).

4. Dynamics of the condensate

When $\ell_{\rm max} = aL$, there are two different regimes of condensate dynamics. At densities ρ just above the transition density $\rho_{\rm trans}$, the system occasionally switches to the disordered metastable state with $m = 0$. In this regime, the condensate dissolves, the system spends some time in a disordered state with no condensate, and then another condensate forms on a random site. At higher densities, the behavior is similar to that discussed in Sec. IV A 3: a new condensate begins to form two sites ahead of the condensate (at site 3 if the condensate is located at site 1) while the old condensate still exists. The probabilities of both types of events (condensate "melting" and condensate relocation to the next-nearest neighbor) vanish exponentially with the system size, but with different exponential rates which depend on ρ and a. In the thermodynamic limit the less improbable of the two events dominates and dictates the typical condensate motion regime. The two dynamical regimes are separated by a sharp dynamical phase transition, at a density which can in principle be computed from $I^{(2)}_\rho(m, m_2)$ [45].

C. Further comments about the condensed phase

Two final remarks about the condensed phase. First, note that the mean current in the condensed phase is the sum of the rate with which a particle hops to the next site, plus twice the rate with which it hops two sites. Therefore,

$$\begin{aligned} J_i &= [1 - P_i(0)]P_{i+1}(0) + 2[1 - P_i(0)][1 - P_{i+1}(0)] \\ &= [1 - P_i(0)][2 - P_{i+1}(0)], \end{aligned} \tag{32}$$

For all sites but a few which are close to the condensate this current is approximately $J \simeq [1 - q_\infty][2 - q_\infty] = 1$. This implies that the current in the corresponding AEP is $J_{\rm AEP} = 1 - \rho_{\rm AEP}$, as found in Ref. [14].

A second remark concerns the single site occupation probability $P(n)$, i.e., the probability the an arbitrary site has n particles. According to the analysis presented above, on a finite system of size L, for $n < \ell_{\rm max}$ this probability decays exponentially as $P(n) \sim [q^n_\infty + L^{-1}q^n_3]$, while for $n > \ell_{\rm max}$ it has a peak around $N_{\rm cond} = L(\rho - \rho_c)$ due to the condensate. In between, we expect a plateau which reflects the times in which there are two (next-nearest neighbor) sites competing to be the condensate. The hight of this plateau should be of order $O[q_3^{\ell_{\rm max}}/(\rho - \rho_c - a)]$, where $a = \lim_{L\to\infty} \ell_{\rm max}/L$. The reason for this scaling is that the probability to see two condensate sites is approximately $T_{\rm takeover}/T_{\ell_{\rm max}} = O(L^2 q_3^{\ell_{\rm max}})$, the probability that a given site is one of these two condensates is $2/L$, and when there are two condensate sites all $L(\rho - \rho_c - a)$ occupation values between $\ell_{\rm max}$ and $N_{\rm cond} - \ell_{\rm max}$ are equally probable.

V. NUMERICAL SIMULATIONS

In this section, we present results of numerical simulations of the AEP, and compare them to the MF predictions discussed above. We find that simulation results qualitatively follow the MF predictions, even though there are quantitative discrepancies between the two. Furthermore, the numerical measurements of the LDF $I_\rho(m)$ and of the phase diagram quantitatively agree, to a rather high accuracy, with the MF theoretical predictions. This quantitative agreement is somewhat surprising, as the MF approximation is expected to be inexact and hold only on a qualitative level. We do not, however, have enough numerical data to determine whether the MF phase diagram is indeed exact.

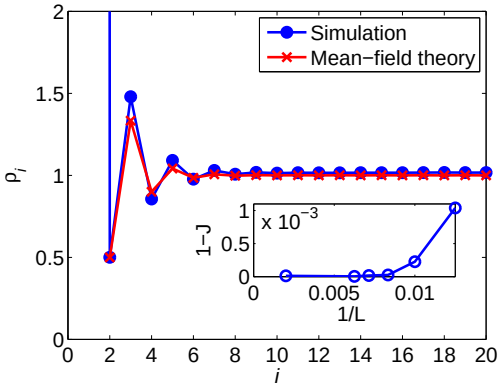

FIG. 6. Numerical results and MF predictions for the mean density profile as seen from the condensate. The condensate is located at site 1 (by definition of the site labels). Simulation results are for $a = 0.15$, $\rho = 4$ and $L = 160$. A good qualitative agreement is observed. In the inset, the mean current J is seen to approach $J = 1$, the MF predicted value, when the system size is increased. Results are for $a = 0.15$, $\rho = 4$, and various system sizes between $L = 80$ and $L = 500$.

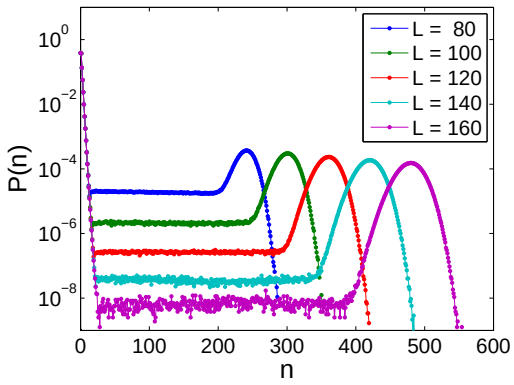

FIG. 7. (Color Online) The single-site occupation probability $P(n)$ in the condensed phase as measured in simulations. L increases from top to bottom. The peak due to the condensate is clearly seen. The plateau at intermediate values of n is a consequence of events in which the condensate relocates to a different site, as discussed in Sec. IV C. Here $a = 0.15$, $\rho = 4$.

We focus in this section on simulations of the case with a first-order phase transition, $\ell_{\max} = aL$. The other case, of $\log L \lesssim \ell_{\max} \ll L$ is equivalent to the limit of $a \to 0$ of the case we focus on.

A. Typical behavior in the condensed phase

We begin by examining the typical behavior of the AEP in the condensed phase. First, we measure the mean density profile as seen from the condensate: we label the position of the most occupied site as 1, and measure $\rho_i = \langle n_i \rangle$ for $i = 1, \ldots, L$. Here $\langle \cdot \rangle$ denotes an average in the steady state. In Fig. 6, numerical results are compared with the MF values calculated in Sec. IV A 2. A good qualitative agreement is found. In particular, the density profile is seen to depend on the distance from the condensate — the basic fact which underlies the condensate drift — and furthermore the density oscillates and decays exponentially with the distance to a value $\rho_\infty \approx 1$. As expected, there are quantitative discrepancies between the MF approximation and the simulation results. Note that we have measured a small deviation $\rho_\infty \simeq 1.017$ (obtained for $a = 0.15$ and $\rho = 4$) from the MF prediction $\rho_\infty = \rho_c = 1$, a deviation smaller than 2%. This deviation does not seem to vanish when increasing the system size up to $L = 500$ (the largest system examined).

In the inset of Fig. 6 we display the mean current $J \equiv L^{-1} \sum J_i$ (where J_i is the mean current leaving site i) and show that it approaches the predicted value $J = [1 - q_\infty][2 - q_\infty] = 1$.

We also plot, in Fig. 7, the single-site occupation probability $P(n)$, i.e., the probability to find n particles in any given site, in the condensed phase. As discussed in Sec. IV C, $P(n)$ is exponentially decaying for small values of n — this is the occupation probability in the fluid background — and has a peak at high values of n due to the condensate. The hight of the plateau in intermediate values of n, which results from condensate relocation events, decays exponentially with the system size, albeit with a different exponent than the MF prediction discussed above (numerical results not reproduced here).

B. Phase diagram and condensate LDF

We move on to examine the phase diagram. Via a finite-size scaling analysis, we have directly measured $\rho_{\rm trans}(a)$ for $a = 0.15$ and $a = 0.5$. The numerical simulations required for this measurement are quite lengthy, as statistics from many switches between the $m = 0$ and $m = \rho - 1$ metastable states are needed, and the typical time between such switches diverges exponentially both with L and with a. The details of the numerical analysis are presented in Appendix D. The results are presented in Fig. 4, where a very good agreement is found between the measurements and the MF values.

The possibility that the MF phase diagram is exact receives stronger support by examining the condensate occupation LDF. Finite size estimates of the LDF,

$$I_\rho(m; L) \equiv -\frac{1}{L} \log \text{Prob}\left(n_{\max} = mL\right), \qquad (33)$$

were measured for several systems sizes at various system parameters, see Fig. 8. A scaling collapse is found, indicating that the condensate occupation indeed satisfies a large deviation principle. Furthermore, there is a good agreement between the MF prediction (29) and this scaling collapse. Since $\rho_{\rm trans}(a)$ is defined by this LDF (it

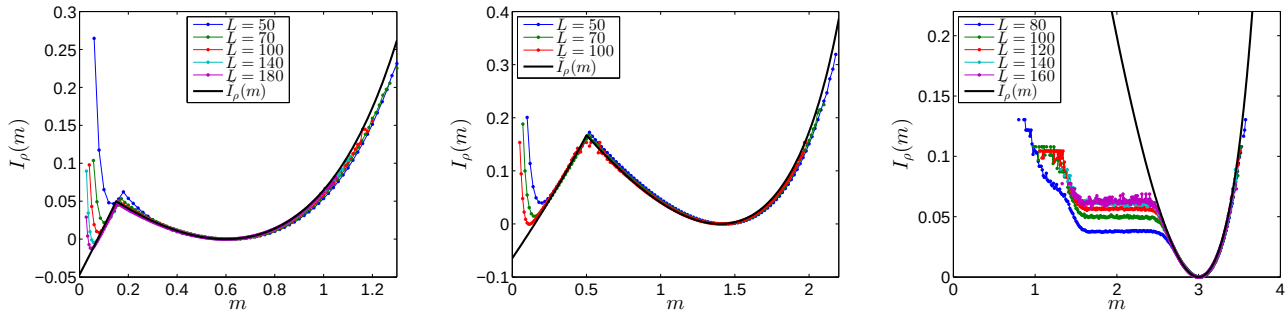

FIG. 8. (Color online) Symbols: the finite-size LDF $I_\rho(m;L)$ [Eq. (33); lines are presented as a guide to the eye], measured numerically at different system sizes. Solid black line: the MF prediction for $\tilde{I}_\rho(m)$ (29) for $L=\infty$. All plots are normalized so that the minimum of the $m>a$ branch lies at $I_\rho(m)=0$. The system size L increases from top to bottom in the left and middle panels and from bottom to top in the right panel. Model parameters are (left) $a=0.15$, $\rho=1.6$; (middle) $a=0.5$, $\rho=2.4$; and (right) $a=0.15$, $\rho=4$. A good agreement is found between the MF predictions and simulation results. At high densities (the right plot), deviations from $\tilde{I}_\rho(m)$ due to the formation of multiple condensates are seen (compare with Fig. 5).

is the density where the two local minima are equal), if the latter is correct to high accuracy so must the former be. Note also that the minimum of the $m>a$ branch is located close to $\rho-1$, in agreement with the predicted edge of stability line $\rho=a+1$. One caveat is that, as mentioned above, the background density ρ_∞ in the condensed phase is seen to deviate slightly from the MF value 1. This deviation might indicate that the MF prediction for $I_\rho(m)$ is not exact after all, since the $m>a$ minimum of this LDF must be located at $m=\rho-\rho_\infty$.

C. Dynamics of the condensate

Finally, we study the dynamics of the condensate when $\ell_{\max}=aL$. This is done by recording how the location $i_{\max}$ and occupation $n_{\max}$ of the most occupied site evolve with time. As discussed above, the condensate dynamics is dictated by two competing processes: switching to the disordered metastable state, and condensate relocation to another site. At densities close to $\rho_{\rm trans}(a)$ switching is much faster and thus dominates, while at higher densities switching becomes slower and condensate relocation dominates. Measurements of the dynamics in the two regimes are displayed in Fig. 9. When the condensate relocates it is always seen to reappear in its next-nearest neighbor site thus leading to a condensate drift, as predicted by the MF theory.

VI. SUMMARY AND OUTLOOK

In this paper we have presented a mean-field analysis of the AEP. According to this analysis, a condensation transition takes place in the model, but only when $\ell_{\max}$ increases at least logarithmically with the system size. The critical density and current which are found in this case are in agreement with the numerical results presented here and in Ref. [39]. Unlike naive MF approximations, the MF scheme employed here (following Ref. [29]) takes into account some of the effects of spatial correlations in the steady state. We thus find that in the condensed phase, the fluid background is not homogeneous: the mean occupation of a site and its fluctuations depend on the distance from the condensate. As a result, there is, in the thermodynamic limit, an overwhelming probability that when the condensate relocates it does so to its next-nearest neighbor downstream. Therefore, in the slow timescale of the condensate dynamics, it drifts steadily along the lattice. Note that the drift velocity of the condensate in the AEP decays at least algebraically with the system size L, and in particular when $\ell_{\max}=aL$ it decays exponentially with L. This is a much faster decay than the L^{-1} decay of the drift velocity in the model analyzed in Refs. [29, 31].

In the analysis presented above we have made two assumptions that we are not able to justify a-priori. The central one is the MF approximation, which, as is usually the case, is uncontrolled. A second assumption, made during the calculation of the condensate LDF when $\ell_{\max}=aL$, is that the condensate evolution is adiabatic, in the sense that the fluid background is always in its steady state with the momentary condensate occupation (see Sec. IV B 1). To verify the validity of our results, we have compared them with numerical simulations of the model, and have found a good qualitative agreement between the theoretical predictions and numerics. Furthermore, the numerical results agree also quantitatively to a high degree with the predicted MF critical density and current when $\ell_{\max}\ll L$, and with the MF phase diagram when $\ell_{\max}=aL$. It is not yet known whether these MF predictions are exact. Analyzing the model beyond MF approximations is an interesting, and undoubtfully difficult, open problem.

The current work joins Refs. [29, 31] in demonstrating that a condensate drift is a rather generic phenomenon in spatially-correlated nonequilibrium systems where a con-

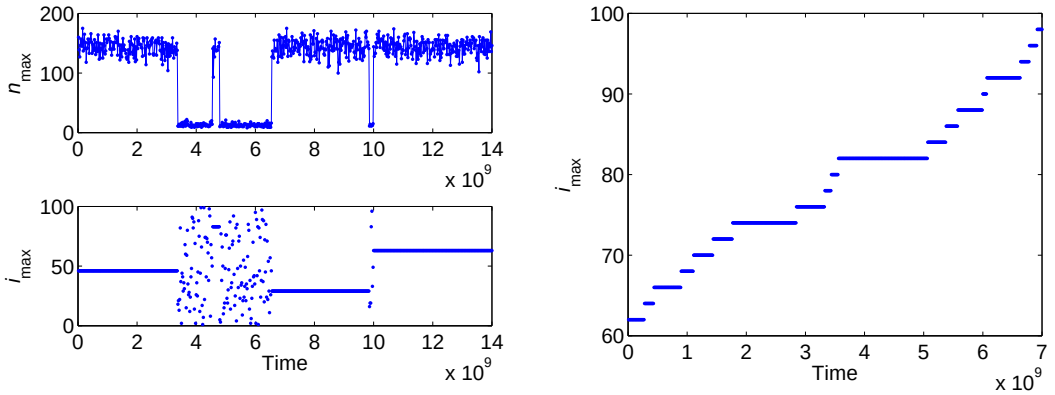

FIG. 9. The dynamics of the condensate. Left panel: slightly above the transition density, the condensate typically relocates to a random site by switching between the condensed and disordered metastable states. Here we plot the occupation (top) and location (bottom) of the most occupied site as a function of time, in a system with $L = 100$, $a = 0.5$, and $\rho = 2.44$. Note that this density is somewhat below $\rho_{\rm trans}(a)$, but it is above its finite-size counterparts $\rho_{\rm trans}(a; L)$, see Appendix D. Right panel: at higher densities, the condensate typically relocates to its next nearest neighbor [the occupation $n_{\rm max}$, not plotted here, fluctuates around $(\rho - 1)L$]. Here $L = 160$, $a = 0.15$, and $\rho = 4$. Note the scale of the time axes.

densate spontaneously breaks the translation symmetry. It would be interesting to study from a more general perspective the symmetry-breaking aspect of the drift mechanism. Recently, a similar emergent motion was found in a system where a different symmetry is spontaneously broken: a phase with a rotating magnetization was established in a driven XY model [48]. It would be very interesting to find other systems that exhibit a motion induced by the combination of spontaneous symmetry breaking and a drive, and to ascertain how general this phenomenon is.

ACKNOWLEDGMENTS

We thank A. Bar, O. Cohen, T. Sadhu, and R. K. P. Zia for useful discussions. The support of the Israel Science Foundation (ISF) and of the Minerva Foundation with funding from the Federal German Ministry for Education and Research is gratefully acknowledged.

Appendix A: Bulk properties in the condensed phase when $\ell_{\rm max} \ll L$

In this appendix, we complete the details of the calculation of $P_i(0)$, q_i, and Q_i in the condensed phase. Assuming that no site other than the condensate has more than $\ell_{\rm max}$ particles, one obtains Eq. (22) from Eqs. (7) and (11). As shown in Sec. IV A 2, the boundary condition for this recursion relation is $P_2(0) = 1/2$ and $P_3(0) = 1/3$.

Calculating the next few terms in the sequence yields

$$P_4(0) = \frac{2}{5}, \qquad P_5(0) = \frac{3}{8}, \quad \text{and} \quad P_6(0) = \frac{5}{13}, \tag{A1}$$

leading us to guess $P_i(0) = F_{i-1}/F_{i+1}$, where F_i is the i'th Fibonacci number. We prove this guess by induction: substituting our guess in the right hand side of Eq. (22) yields

$$P_{i+1}(0) = \frac{1 - [1 - P_i(0)][1 - P_{i-1}(0)]}{2 - P_i(0)} = \frac{1 - \left[\frac{F_i}{F_{i+1}}\right]\left[\frac{F_{i-1}}{F_i}\right]}{2 - \frac{F_{i-1}}{F_{i+1}}} = \frac{\frac{F_{i+1}-F_{i-1}}{F_{i+1}}}{\frac{F_{i+1}+(F_{i+1}-F_{i-1})}{F_{i+1}}} = \frac{F_i}{F_{i+2}}, \tag{A2}$$

where we have repeatedly used $F_{i+1} - F_{i-1} = F_i$.

Finally, substituting in (7) yields $q_i = F_{i-2}/F_i$ and $Q_i = 1$.

Appendix B: Fixed point analysis of Eq. (22)

In this Appendix, we analyze the fixed points of the recursion relation for $P_i(0)$, Eq. (22). To simplify notation, we denote in this Appendix

$$p_i \equiv P_i(0). \tag{B1}$$

First, we rewrite the second order recursion relation (22) as a two-dimensional first order one

$$(p_{i+1}, p_i) = f(p_i, p_{i-1}), \text{ with } f(x, y) = \left(y, \frac{x + y - xy}{2 - y}\right). \tag{B2}$$

The map (B2) has a one-parameter family of fixed points, the line $x = y$. Therefore, any value of p_i is a fixed point of the map.

Denote by $d(x, y) \equiv (y - x)/\sqrt{2}$ the signed distance of the point (x, y) from the fixed point line. By signed distance we mean that $|d(x, y)|$ is the Euclidian distance, and d is positive if the point is above the line $(y > x)$ and

negative if it is below it ($y < x$). A simple calculation shows that

$$d\big(f(x,y)\big) = -\frac{1-y}{2-y}\,\frac{y-x}{\sqrt{2}} = -\frac{1-y}{2-y}\,d(x,y). \qquad \text{(B3)}$$

Since $0 \le (1-y)/(2-y) \le 1/2$ for all physical values $0 \le y \le 1$, the distance shrinks by more than a factor of $1/2$ with each iteration of the map. Therefore, the map is an exponential contraction, in the sense that any initial point (x,y) with $0 \le x,y \le 1$ approaches the line $x = y$ exponentially rapidly. It is also seen that consecutive iterations oscillate between the two sides of the fixed point map, i.e., $P_i(0)$ decays to its limiting value via oscillations.

Appendix C: Equation for the LDF of the two most occupied sites

In this Appendix we discuss the equation for the LDF of the occupation of the two most occupied sites. Denote $P^{(2)}_{\max}(mL, m_2L) \equiv P(n_{\max} = mL, n^{(2)}_{\max} = m_2L)$, where $n_{\max}$ is the occupation of the most occupied site and $n^{(2)}_{\max}$ is the second most occupied site. The probability $P^{(2)}_{\max}$ satisfies a master equation similar to (18). Substituting the LDF ansatz

$$P^{(2)}_{\max}(mL, m_2L) \sim e^{-LI^{(2)}_\rho(m,m_2)}, \qquad \text{(C1)}$$

keeping the leading order in L and examining the steady state leads to

$$\begin{aligned} 0 = &\big(1 - e^{\partial_1 I^{(2)}_\rho(m,m_2)}\big)\big[e^{-\partial_1 I^{(2)}_\rho(m,m_2)} - J_{\rm in}(m,m_2)\big] + \\ &\big(1 - e^{\partial_2 I^{(2)}_\rho(m,m_2)}\big)\big[e^{-\partial_2 I^{(2)}_\rho(m,m_2)} - J^{(2)}_{\rm in}(m,m_2)\big], \end{aligned} \qquad \text{(C2)}$$

where $\partial_1 = \partial/\partial m$, $\partial_2 = \partial/\partial m_2$, $J_{\rm in}$ is the current into the most occupied site, and $J^{(2)}_{\rm in}$ is the current into the second most occupied site [49]. In Eq. (C2) we have already used the fact that the current out of both highly occupied sites condensate is 1. This equation must be supplemented by boundary conditions, which are derived from the boundary conditions of the master equation for $P^{(2)}_{\max}$. In particular, when $m_2 = 0$, one finds that $\tilde{I}_\rho(m) \equiv I^{(2)}_\rho(m,0)$ satisfies Eq. (20) with (24) and (27).

A simple solution of the PDE (C2) may be found if each of the two terms in the square brackets vanishes independently. A necessary and sufficient condition for this to occur (found by equating the mixed second derivatives of $I^{(2)}_\rho$) is that

$$\partial_2 \log J_{\rm in}(m,m_2) = \partial_1 \log J^{(2)}_{\rm in}(m,m_2). \qquad \text{(C3)}$$

Unfortunately, a straightforward calculation shows that this is not the case for the AEP.

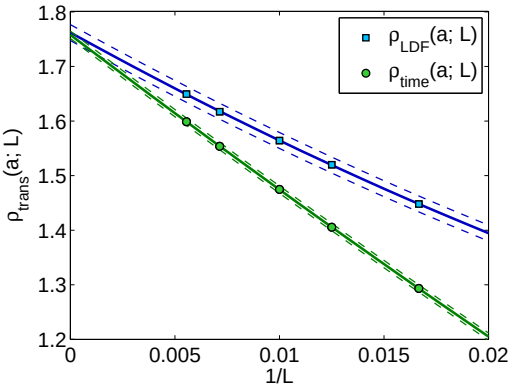

FIG. 10. The transition density $\rho_{\rm trans}(a)$ is estimated by extrapolating the finite-size estimators $\rho_{\rm LDF}(a;L)$ and $\rho_{\rm time}(a;L)$ to $L = \infty$. Markers are simulation measurements and lines are the best fits to a quadratic polynomial in $1/L$. Dashed lines mark the 95% confidence intervals of the fits. The two different estimators agree to within measurement accuracy.

Appendix D: Numerical determination of the transition density

To numerically estimate the transition density $\rho_{\rm trans}(a)$ of Fig. 4 from Monte-Carlo simulation data, we have used a finite-size scaling analysis. In this Appendix we explain our calculational procedure. The analysis is based on measuring finite-size estimators of the critical density, and extrapolating these measurements to $L = \infty$.

We study two natural finite-size estimators for $\rho_{\rm trans}(a)$.

(i) We define $\rho_{\rm LDF}(a;L)$ as the density at which the two local minima of the finite-size LDF $I_\rho(m;L)$ [Eq. (33)] have the same value (see Fig. 8). Denote the location of the left minimum for a given values of L and a by m^*_l and of the right by m^*_r. Then $\rho_{\rm LDF}(a;L)$ is defined by

$$I_{\rho_{\rm LDF}(a;L)}(m^*_l;L) = I_{\rho_{\rm LDF}(a;L)}(m^*_r;L). \qquad \text{(D1)}$$

Note that for a given value of L the density ρ can only change by multiples of $1/L$, and thus there may not by a "legitimate" density at which this equality holds. In this case, we interpolate results to densities which are not multiples of $1/L$. Thus, $\rho_{\rm LDF}(a;L)$ need not be a multiple of $1/L$.

(ii) As an alternative finite-size estimator, we define $\rho_{\rm time}(a;L)$ as the density at which the system spends an equal fraction of the time in each of the two metastable states. To this end we measure the fraction of time $p_{\rm dis}(\rho)$ that the system is in the disordered state, i.e., $p_{\rm dis}(\rho) \equiv {\rm Prob}(n_{\max} \le \ell_{\max})$. Then, $\rho_{\rm time}(a;L)$ is defined by

$$p_{\rm dis}\big(\rho_{\rm time}(a;L)\big) = 1/2. \qquad \text{(D2)}$$

Here too we interpolate $p_{\rm dis}(\rho)$ to densities which are not multiples of $1/L$.

Both of these estimators converge to $\rho_{\rm trans}(a)$ when $L \to \infty$. At large system sizes, the second estimator can be measured to a somewhat higher accuracy, because at the density $\rho_{\rm LDF}(a;L)$ the systems spends a small fraction of the time in the disordered state, and thus more statistics (i.e., longer simulation times) are needed in order to estimate $I_\rho(a;L)$ to a high enough accuracy.

Next, we assume that both estimators can be expanded around $L=\infty$ as $\rho_{\rm trans}(a;L) = \rho_{\rm trans}(a) + c_1/L + c_2/L^2 + \ldots$ for some coefficients c_i, where $\rho_{\rm trans}(a;L)$ stands for either of the two estimators. We then fit the measured values to a quadratic function in $1/L$, and extract the transition density, see Fig. 10. We estimate the error as the 95% confidence intervals of the fit; this in fact somewhat underestimates the error, as it does not take into account the statistical and systematic errors on the estimation of $\rho_{\rm trans}(a;L)$ (the latter are due to the interpolation discussed above).

[1] M. R. Evans and T. Hanney, J. Phys. A **38**, R195 (2005).

[2] S. N. Majumdar, in *Exact Methods in Low-Dimensional Statistical Physics and Quantum Computing: Lecture Notes of the Les Houches Summer School July 2008*, Vol. 89, edited by J. Jacobsen *et al.* (Oxford University Press, Oxford, 2010) arXiv:0904.4097v1.

[3] A. Schadschneider, D. Chowdhury, and K. Nishinari, *Stochastic Transport in Complex Systems: From Molecules to Vehicles* (Elsevier Science, Amsterdam, 2010).

[4] S. N. Dorogovtsev and J. F. F. Mendes, *Evolution of Networks* (Oxford University Press, Oxford, 2003); S. N. Dorogovtsev, A. V. Goltsev, and J. F. F. Mendes, Rev. Mod. Phys. **80**, 1275 (2008).

[5] K. van der Weele, D. van der Meer, M. Versluis, and D. Lohse, Europhys. Lett. **53**, 328 (2001).

[6] J. P. Bouchaud and M. Mézard, Physica A **282**, 536 (2000).

[7] S. N. Majumdar, S. Krishnamurthy, and M. Barma, Phys. Rev. Lett. **81**, 3691 (1998).

[8] M. R. Evans, Brazilian Journal of Physics **30**, 42 (2000).

[9] Y. Kafri, E. Levine, D. Mukamel, G. M. Schütz, and J. Török, Phys. Rev. Lett. **89**, 035702 (2002).

[10] T. Hanney and M. R. Evans, Phys. Rev. E **69**, 016107 (2004).

[11] S. N. Majumdar, M. R. Evans, and R. K. Zia, Phys. Rev. Lett. **94**, 180601 (2005).

[12] M. R. Evans, T. Hanney, and S. N. Majumdar, Phys. Rev. Lett. **97**, 010602 (2006).

[13] B. Waclaw, J. Sopik, W. Janke, and H. Meyer-Ortmanns, Phys. Rev. Lett. **103**, 080602 (2009); J. Stat. Mech. **2009**, P10021 (2009).

[14] S. Grosskinsky and G. M. Schütz, J. Stat. Phys. **132**, 77 (2008).

[15] S. Grosskinsky, F. Redig, and K. Vafayi, J. Stat. Phys. **142**, 952 (2011).

[16] C. Godrèche and J. M. Luck, J. Stat. Mech. **2012**, P12013 (2012).

[17] H. Sachdeva, M. Barma, and M. Rao, Phys. Rev. Lett. **110**, 150601 (2013); H. Sachdeva and M. Barma, J. Stat. Phys. **154**, 950 (2014).

[18] J. Szavits-Nossan, M. R. Evans, and S. N. Majumdar, Phys. Rev. Lett. **112**, 020602 (2014); J. Phys. A **47**, 455004 (2014).

[19] M. Filiasi, E. Zarinelli, E. Vesselli, and M. Marsili, ArXiv e-prints (2013), arXiv:1309.7795 [cond-mat.stat-mech]; M. Filiasi, G. Livan, M. Marsili, M. Peressi, E. Vesselli, and E. Zarinelli, J. Stat. Mech. **2014**, P09030 (2014).

[20] P. Chleboun and S. Grosskinsky, J. Stat. Phys. **154**, 432 (2014).

[21] R. J. Concannon and R. A. Blythe, Phys. Rev. Lett. **112**, 050603 (2014).

[22] A. Bar and D. Mukamel, Phys. Rev. Lett. **112**, 015701 (2014); J. Stat. Mech. **2014**, P11001 (2014).

[23] J. Kaupužs, R. Mahnke, and R. J. Harris, Phys. Rev. E **72**, 056125 (2005).

[24] Z. Burda, J. D. Correia, and A. Krzywicki, Phys. Rev. E **64**, 046118 (2001); S. N. Dorogovtsev, J. F. F. Mendes, and A. N. Samukhin, Nuclear Physics B **666**, 396 (2003); A. G. Angel, M. R. Evans, E. Levine, and D. Mukamel, Phys. Rev. E **72**, 046132 (2005); A. G. Angel, T. Hanney, and M. R. Evans, Phys. Rev. E **73**, 016105 (2006).

[25] J. Török, Physica A **355**, 374 (2005).

[26] Z. Burda, D. Johnston, J. Jurkiewicz, M. Kamiński, M. A. Nowak, G. Papp, and I. Zahed, Phys. Rev. E **65**, 026102 (2002).

[27] R. Rajesh and S. N. Majumdar, Phys. Rev. E **63**, 036114 (2001).

[28] R. Rajesh and S. Krishnamurthy, Phys. Rev. E **66**, 046132 (2002).

[29] O. Hirschberg, D. Mukamel, and G. M. Schütz, Phys. Rev. E **87**, 052116 (2013).

[30] C. Godrèche and J. M. Luck, J. Phys. A **38**, 7215 (2005).

[31] O. Hirschberg, D. Mukamel, and G. M. Schütz, Phys. Rev. Lett. **103**, 090602 (2009); J. Stat. Mech. **2012**, P08014 (2012).

[32] B. Waclaw and M. R. Evans, Phys. Rev. Lett. **108**, 070601 (2012); J. Phys. A **47**, 095001 (2014).

[33] J. Beltran and C. Landim, Probability Theory and Related Fields **152**, 781 (2012).

[34] C. Landim, Commun. Math. Phys. **330**, 1 (2014).

[35] P. Chleboun and S. Grosskinsky, J. Phys. A **48**, 055001 (2015).

[36] J. Whitehouse, A. Costa, R. A. Blythe, and M. R. Evans, J. Stat. Mech. **2014**, P11029 (2014).

[37] I. Armendáriz, S. Grosskinsky, and M. Loulakis, ArXiv e-prints (2015), arXiv:1507.03797 [math.PR].

[38] Y.-X. Chau, C. Connaughton, and S. Grosskinsky, ArXiv e-prints (2015), arXiv:1508.07516 [cond-mat.stat-mech].

[39] J. Dong, S. Klumpp, and R. K. P. Zia, Phys. Rev. Lett. **109**, 130602 (2012).

[40] J. Dong, S. Klumpp, and R. K. P. Zia,

Phys. Rev. E **87**, 022146 (2013).
[41] J. Merikoski, Phys. Rev. E **88**, 062137 (2013).
[42] U. Bhat and P. L. Krapivsky, Phys. Rev. E **90**, 012133 (2014).
[43] T. Dauxois, S. Ruffo, and L. Cugliandolo, eds., *Long-Range Interacting Systems*, Lecture Notes of the Les Houches Summer School, Vol. 90 (Oxford University Press, 2009).
[44] T. Dauxois and S. Ruffo, eds., *Topical Issute: Long-Range Interacting Systems*, J. Stat. Mech. (2011).
[45] P. I. Chleboun, *Large deviations and metastability in condensing stochastic particle systems*, Ph.D. thesis, University of Warwick (2011).
[46] If $P(n_{\max} = mL) \sim e^{-LI(m)}$ then $I(m)$ is called the large-deviation function or rate function of $n_{\max}$; see [50] for an introduction to the theory of large deviations. Throughout the paper we use the symbol $\sim$ to denote exponential equivalence to leading order in L. For example, the above relation means that $I(m) = \lim_{L\to\infty} L^{-1} \log P(n_{\max} = mL)$.
[47] More precisely, for any system of finite size L, the maximal occupation in the homogeneous fluid background is of order $\log L$ (as this is the maximum of $O(L)$ independent random variables whose distribution has an exponential tail). Therefore, $J_{\text{out}}(n_{\max}/L)$ decreases from 1 to 0 as $n_{\max}$ decreases from some value of order $\log L$ to 0. Thus, the other locally stable fixed point is at $m = O(\log L/L) \to 0$ when $L \to \infty$.
[48] C. Maes and S. Shlosman, J. Stat. Phys. **144**, 1238 (2011).
[49] The explicit forms of J_{in} and $J_{\text{in}}^{(2)}$ will not be important for us and so we do not write them here. $J_{\text{in}}(m, m_2)$ is similar to (24) with $\rho_{\text{bg}} = \rho - m - m_2$; $J_{\text{in}}^{(2)}(m, m_2)$ also has a similar form, but with q_∞ and Q_∞ replaced by q_3 and Q_3.
[50] H. Touchette, Phys. Rep. **478**, 1 (2009).